minerals

MDPI

Article

Influence of Amino Acids on the Mobility of Iodide in Hydrocalumite

Mengmeng Wang [1], Hirofumi Akamatsu [2] and Keiko Sasaki [1,*]

[1] Department of Earth Resources Engineering, Kyushu University, Fukuoka 819-0395, Japan; wang@mine.kyushu-u.ac.jp
[2] Department of Applied Chemistry, Kyushu University, Fukuoka 819-0395, Japan; h.akamatsu@cstf.kyushu-u.ac.jp
* Correspondence: keikos@mine.kyushu-u.ac.jp

Abstract: In the cement system, hydrocalumite is a candidate adsorbent for low-level ^{129}I anionic species. However, the stability of hydrocalumite after immobilizing I^- is unclear when they are exposed to pedosphere characterized by organic substances derived from living organisms. In the present work, five amino acids were selected as simplified models of natural organic substances under alkaline conditions. L-cysteine (H_2Cys) and L-aspartic acid (H_2Asp) accelerated the release of I^- from I-hydrocalumite through ion-exchange. Ion-exchange of Cys^{2-} with I^- in I-hydrocalumite was faster than Asp^{2-}, and the interlayer spacing (d_{003}) of Cys-hydrocalumite was smaller than that of Asp-hydrocalumite. DFT simulations not only supported the above results but also predicted that there was a positive correlation between the formation energies and interlayer spacings of amino acids intercalated hydrocalumite, depending on the configurations. Moreover, in the DFT predictions, the interaction between amino acids and metallic hydroxide layers was responsible for the formation of hydrogen bonds and Ca-O chemical bonds between the -COO^- groups and $[Ca_2Al(OH)_6]^+$. The other three amino acids did not show intercalation through ion-exchange. The stability of I-hydrocalumite is influenced differently by coexisting amino acids, depending on the ionic sizes, charge numbers, and hydrophilicity, which cause the second contamination.

Keywords: iodide; hydrocalumite; amino acids; DFT simulation; simple dissolution; ion-exchange

Citation: Wang, M.; Akamatsu, H.; Sasaki, K. Influence of Amino Acids on the Mobility of Iodide in Hydrocalumite. *Minerals* **2021**, *11*, 836. https://doi.org/10.3390/min11080836

Academic Editor: Gianfranco Ulian

Received: 14 June 2021
Accepted: 27 July 2021
Published: 1 August 2021

1. Introduction

In the process of cement hydration, tricalcium aluminate, $Ca_3Al_2O_6$ (C_3A), is one of the most reactive substances, and several hydrated phases, such as SO_4-ettringite ($3CaO{\cdot}Al_2O_3{\cdot}3CaSO_4{\cdot}32H_2O$) and SO_4-hydrocalumite ($3CaO{\cdot}Al_2O_3{\cdot}CaSO_4{\cdot}12H_2O$), can be formed [1–3]. Among them, hydrocalumite is one of the layered double hydroxides (LDHs) that is well known to immobilize anionic species due to its positively charged surfaces and large ion-exchange capacities [4–6]. The low-level radioactive anionic species can be immobilized in a cement matrix, which could be stored in a relatively shallow underground zone under anoxic conditions.

^{129}I possesses a half-life of 1.57×10^7 years and is generally produced by nuclear power plants, which can be extremely hazardous to the pedosphere and human health in the long term [7–9]. Under anoxic repository conditions, ^{129}I shows a stable iodide (I^-) form which cannot be directly precipitated like iodate (IO_3^-) [10]. Therefore, it is highly mobile in the pedosphere. Hydrocalumite plays an important role in I^- immobilization through surface adsorption and incorporation into structures, suggesting that hydrocalumite can be a good candidate for the stabilization of I^- in Portland cement systems [11,12]. Aimoz et al. [13] found that SO_4-hydrocalumite can take up I^-. However, the stability of hydrocalumite after immobilizing I^- is of concern for a deeper understanding of the effectiveness of cement stabilization/solidification (S/S).

The stability of I^- in the hydrocalumite interlayer is always seriously affected by its coexistence with other anions, which have higher affinities with hydrocalumite. In contaminated soil or water systems, there are a variety of coexisting inorganics and organic ions, which possibly come into contact with cementitious materials after immobilizing target pollutants [14–17]. Generally, the effects of major inorganic ions, such as Cl^-, OH^-, CO_3^{2-}, and SO_4^{2-}, in environments on the stability of hydrocalumite have been explored. Aimoz et al. [13] explored the retention behavior of I^- in the hydrocalumite phase, and found that Cl^- and CO_3^{2-} showed a competitive relationship with I^- to intercalate into the hydrocalumite interlayer and reduced the stability of I-hydrocalumite and SO_4-hydrocalumite. Nedyalkova et al. [18] also confirmed that the capability of hydrocalumite bearing I^- became weak due to the formation of monocarbonate as the reaction time went on. The selectivity of anions in hydrocalumite is important to immobilize anionic pollutants in the environment. In environmental mineralogy, the effect of organic substances cannot be ignored because they are abundant in the pedosphere. However, the effects of organic substances on the stability of I-hydrocalumite have not yet been explored. Amino acids are monomers of proteins that exist in free single molecules and degradation products of soil, small animals, plants, and microorganisms. Natural amino acids contain amine (-NH_2) and carboxyl (-COOH) groups and can be classified into hydrophobic, neutral, and hydrophilic groups depending on their specific side chains (R group). Some amino acids can be charged to −2 due to their two carboxyl groups and the existence of a thiol group. Therefore, to some extent, the chemical properties of amino acids can represent complicated natural organic substances as models [19].

In the current work, I-hydrocalumite was prepared through co-precipitation. Five amino acids were selected to explore the stability of I-hydrocalumite, considering the molecular sizes, charge numbers, functional groups, and hydrophilicity. Based on Ca and Al oxide hydration under alkaline conditions, the released behavior of I^-, adsorption behavior of amino acids, and solid residue phase changes were elaborated. Density functional theory (DFT) simulations were applied to determine the possible configurations and support the experimental results and the possible release mechanisms of I^- in the presence of amino acids.

2. Materials and Methods

2.1. Reagents

All reagents used in the present work were purchased from Wako Chemicals (Osaka, Japan). Inorganic reagents including $CaCO_3$ (98%), Al_2O_3 (99%), NaOH (97%), and $CaI_2{\cdot}nH_2O$ (99.5%) were of analytical grade.

There are 20 types of amino acids that exist in nature. Depending on their specific side chain groups, they can be classified as hydrophilic, hydrophobic, and amphipathic. L-phenylalanine (HPhe, $C_9H_{11}NO_2$, 99%) and L-tryptophan (HTrp, $C_{11}H_{12}N_2O_2$, 99%) have aromatic groups that make them more hydrophobic than L-cysteine (H_2Cys, $C_3H_7NO_2S$, 99%), L-aspartic acid (H_2Asp, $C_4H_7NO_4$, 99%), and glycine (HGly, $C_2H_5NO_2$, 99%), which have hydrophilic side chain groups. Each amino acid has different acid dissociation constants (pK_a); depending on the relationship between the solution pH and pK_a, the different negative charge numbers for each amino acid can be produced. Under the present experimental conditions, where pH was higher than 12.0, HGly, HTrp, and HPhe had one negative charge but H_2Cys and H_2Asp had two negative charges. Hence, different behaviors could be expected. H_2Cys, H_2Asp, HGly, HTrp, and HPhe of a special grade were used. For high performance liquid chromatography (HPLC) analyses, phenyl isothiocyanate (PITC, 98%) of a special grade, acetonitrile, methanol, and *n*-hexane of HPLC grade were used. All the solutions were prepared using decarbonized Milli-Q water (integral water purification system, Millipore (Burlington, MA, USA)) that was boiled and purged with N_2 gas for 2 h.

2.2. Synthesis of I-Hydrocalumite

Tricalcium aluminate, $Ca_3Al_2O_6$ (C_3A), was prepared by the calcination of a mixture of 30.027 g of $CaCO_3$ and 10.196 g of Al_2O_3 at a molar ratio of 3:1 for 72 h at 1300 °C in a furnace [11,20]. Thereafter, the obtained solid was obtained for the following experiments. I-hydrocalumite, $Ca_4Al_2(OH)_{12}I_2{\cdot}4H_2O$, was prepared by co-precipitation using 0.02 mol C_3A and 0.02 mol $CaI_2{\cdot}nH_2O$, stirring at 600 rpm in a glovebox (95% N_2, 5% H_2, COY, M-160, Grass Lake, MI, USA) to avoid carbon dioxide (CO_2) contamination. After 72 h, the suspension was centrifuged to separate the solid residues, which were rinsed with decarbonized water, freeze-dried for 24 h, and then stored for further use.

2.3. Reaction with Amino Acids

A total of 50 mg of synthesized I-hydrocalumite were suspended in 50 mL of solutions, with and without 1.7 mM amino acids. The initial pH of each solution was adjusted to pH 12.0 using 3 M NaOH. A pH of 12.0 was selected to simulate the alkalinity conditions of a real cement system. The suspensions were shaken at 100 rpm in polyethylene plastic bottles for different time intervals, from 0.5 to 24 h, followed by collection of leaching solutions using disposable syringes and solid residues by filtration using 0.2 µm membrane filters to freeze-drying for 12 h. The solubility of I-hydrocalumite in ultrapure water was evaluated separately without adding amino acids. After reacting with amino acids, the soluble fraction of I^- was evaluated.

2.4. Chemical Analysis and Solid Characterization

Inductively coupled plasma optical emission spectrometry (ICP-OES, Optima 8300, Perkin Elmer, Waltham, MA, USA) was adopted to determine the concentrations of Ca and Al. The concentration of I^- was determined by ion chromatography (IC, ICS-2100, Thermo Scientific, Yokohama, Japan). High-performance liquid chromatography (HPLC, LC-NetII/ADC, Jasco, Hachioji, Japan) was used for determination of the concentrations of amino acids. The solid residues were characterized using X-ray diffraction (Ultima IV XRD Rigaku, Akishima, Japan) using Cu Kα radiation (40 kV, 40 mA, λ = 1.54184 Å) with a Ni filter at a scanning speed of 2°/min and scanning step of 0.02°. The morphology of the hydrocalumite samples, before and after reaction with different amino acids, was observed using a field emission scanning electron microscope (FlexSEM 1000, Hitachi, Tokyo, Japan) at 20 kV. The soluble fraction was calculated based on concentrations of Ca^{2+}, $Al(OH)_4{}^-$, and I^-, following Equation (1):

$$\text{Dissolved fraction (\%)} = C_t/C_0 \times 100 \quad (1)$$

where the C_t (mmol) is the released amount of ions in the solution at time t (h) and C_0 (mmol) is the amount of ions in pristine I-hydrocalumite solid.

2.5. DFT Simulation

Density functional theory (DFT) simulations were applied to predict the intercalation of amino acids, as well as the possible interaction between amino acids and hydrocalumite. Due to the expanded peaks in the XRD patterns that only appeared in the presence of Asp^{2-} and Cys^{2-}, the intercalation behavior of Asp^{2-} and Cys^{2-} may have occurred. Thus, Asp^{2-} and Cys^{2-} were selected as the model amino acids for the DFT simulation.

The projector augmented-wave (PAW) method [21,22] implemented in VASP code [23–25] was employed for the precise description of electronic structures and also due to its low computational costs. The PBEsol-type of exchange-correlation functional within the generalized gradient approximation (GGA) [26–28], combined with D3 van der Waals correction [29,30], was used with the plane-wave cutoff energy of 550 eV. Dispersion forces belonging to van der Waals forces are types of force acting between atoms and molecules that are normally electrically symmetric [31]. Hydrogen bonds are primarily the electrostatic forces of attraction between a hydrogen (H) atom, which is covalently bound

to a more electronegative atom or group, and another electronegative atom with a single pair of electrons [32]. A weak interaction includes electrostatic and dispersion forces. Thus, in the DFT simulation, although H-bonded interactions are dominant, the contribution of dispersion forces is not negligible in computing accurate interaction energies. The states as valence electrons were: 1s for H; 2s and 2p for C, N, and O; 3s and 3p for Al and S; 3p and 4s for Ca.

Initial structural models were prepared as shown in Figure S1, reported in the Supplementary Materials. Firstly, the structural model of positively charged hydroxide layers for Ca_2Al-LDH was constructed for the computer simulations. The hydroxide layers of Ca_2Al-LDH used in the simulations were set using atomic coordinates extracted from the previously reported crystal structure of hydrocalumite with the composition of $[Ca_8Al_4(OH)_{24}(CO_3)(Cl)_2{\cdot}10H_2O]$ [33]. By removing the intercalated carbonate (CO_3^{2-}) and chloride (Cl^-) ions, an "empty" LDH model was created. Since the composition of the LDH layer was $[Ca_2Al(OH)_6]^+$, the number of Al atoms corresponded to the positive charge of the empty LDH model. Secondly, specific Asp^{2-} and Cys^{2-} anions and water molecules were placed in the interlayer spaces of the empty LDH layers at random positions and rotation angles using the pymatgen python library [34] so as to neutralize the positive charge. Thus, more than ten simulated unit cells consisting of the positively charged hydroxide layers of $[Ca_2Al(OH)_6]^+$ and desired intercalated anions were constructed. The relaxation of lattice constants and internal coordinates was performed until the residual stress and force decreased to 4 MPa and 1 meV/Å, respectively. The pymatgen python library was used to extract the structural information such as interlayer spacing and the number of chemical bonds from the optimized structures. The VESTA code was used to visualize the optimized structures [35].

3. Results and Discussion

3.1. Characterizations of Pristine I-Hydrocalumite

Figure 1a,b presents the XRD patterns of the calcined tricalcium aluminate (C_3A, $3CaO{\cdot}Al_2O_3$, PDF#32-0149) and I-hydrocalumite ($3CaO{\cdot}Al_2O_3{\cdot}CaI_2{\cdot}10H_2O$, PDF#042-1474). The solid phase of C_3A is consistent with a previous report [36]. After being co-precipitated with $CaI_2{\cdot}nH_2O$ for 72 h, I-hydrocalumite was formed in a pure phase with a d_{003} value of 8.75 Å at a diffraction angle of 10.10° (2θ), which is consistent with previous reports [13,18]. The molar ratio of Ca/Al is 1.87 is shown in Table 1. Therefore, considering the above results, the formation of I-hydrocalumite is expressed as the following reaction [37] (Equation (2)):

$$3CaO{\cdot}Al_2O_3 + CaI_2 + 10H_2O = Ca_4Al_2(OH)_{12}I_2{\cdot}4H_2O \quad (2)$$

3.2. Effects of Amino Acids on Releasing of I^- from I-Hydrocalumite in Alkaline Solutions

The changes in I^-, Ca^{2+}, $Al(OH)_4^-$, pH, and amino acids at different suspension time intervals are shown in Figure 2. Without any amino acids, after I-hydrocalumite was suspended in an alkaline solution for 0.5 h, and the leaching amount of I^- reached 50.0% of the total amount in pristine I-hydrocalumite. As the reaction time continued, the concentration of the released I^- reached 2.00 mM (91.0%) and the dissolution equilibrium was almost achieved after 6 h. The concentrations of the released Ca (Figure 2b) and Al (Figure 2c) reached 5.37 and 2.78 mM after 24 h, respectively. In addition, the ratios of released Ca/Al were always within 1.85–1.95 which were close to the Ca/Al ratio in pristine I-hydrocalumite. This indicates that the metallic hydroxide layer structure of I-hydrocalumite easily enabled simple dissolution, even though it was under strongly alkaline conditions (Equation (3)).

$$Ca_4Al_2(OH)_{12}I_2{\cdot}4H_2O = 4Ca^{2+} + 2Al(OH)_4^- + 2I^- + 4OH^- + 4H_2O \quad (3)$$

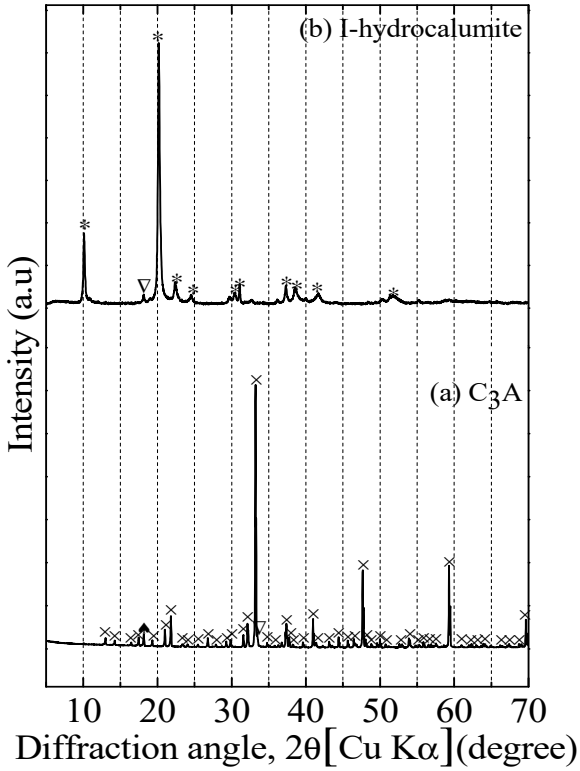

Figure 1. XRD patterns of (**a**) tricalcium aluminate (C_3A); (**b**) I-hydrocalumite. Symbols: ∗, calcium aluminum iodide oxide hydrate ($3CaO{\cdot}Al_2O_3{\cdot}CaI_2{\cdot}10H_2O$, PDF#42-1474); ×, tricalcium aluminate ($3CaO{\cdot}Al_2O_3$, PDF#32-0149); ♠, mayenite ($12CaO{\cdot}7Al_2O_3$, PDF#78-0910); ∇ unknown.

Table 1. Elemental compositions of I-hydrocalumite.

LDHs	Chemical Formula	Ca/mmol·g^{-1}	Al/mmol·g^{-1}	I/mmol·g^{-1}	Ca/Al
I-hydrocalumite	$Ca_{6.0}{\cdot}Al_{3.2}{\cdot}(OH)_{18}{\cdot}(I)_{2.19}{\cdot}6H_2O$	6.0	3.2	2.19	1.87

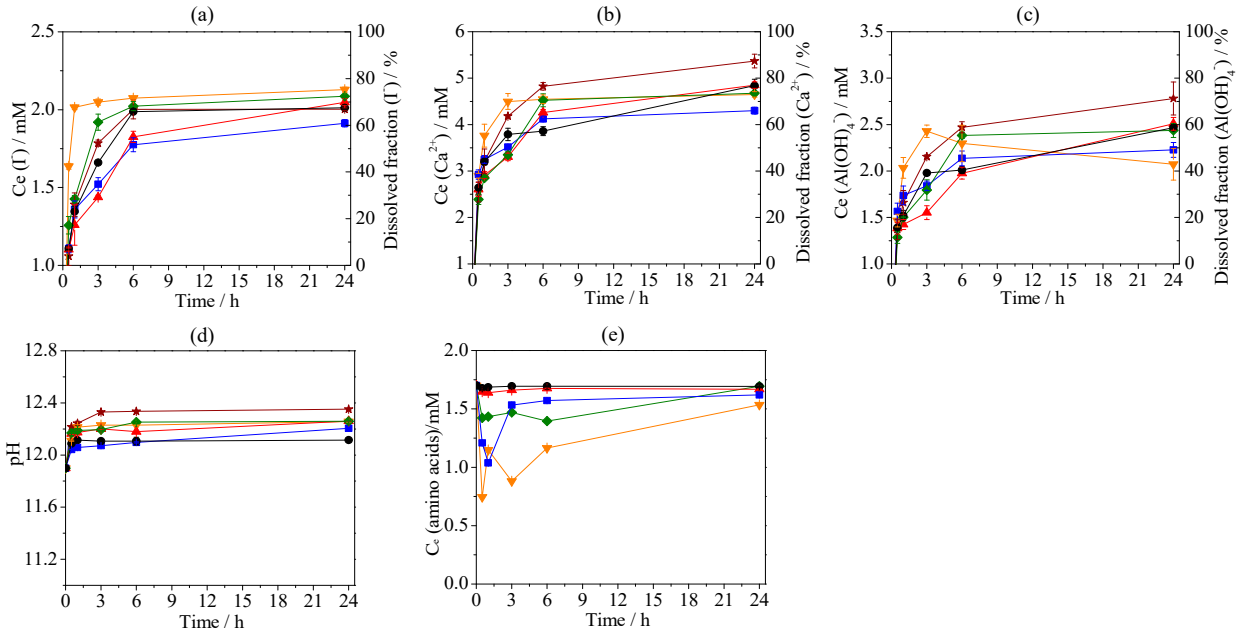

Figure 2. The concentrations of released (**a**) I^-, (**b**) Ca^{2+}, (**c**) $Al(OH)_4^-$, (**d**) pH and (**e**) changing of amino acids at different time intervals. Symbols: ★, Blank; ▲, HGly; ◆, H_2Asp; ▼, H_2Cys; ■, HPhe; ●, HTrp (n = 2).

To verify the dissolution equilibrium, the reactions in this work were continued until the 24 h mark. The XRD patterns of solid residues collected from blank and amino acids tests at different reaction times are presented in Figure 3. Figure 3a shows the results of the blank test, where the phase of I-hydrocalumite was maintained for 3 h, and, after that, it was gradually phase-transferred into the metastable phase of calcium aluminum oxide hydrate ($4CaO{\cdot}Al_2O_3{\cdot}xH_2O$, PDF#02-0077) and $3CaO{\cdot}Al_2O_3{\cdot}xH_2O$, PDF#02-0083). After 6 h, the phase of $4CaO{\cdot}Al_2O_3{\cdot}xH_2O$ completely disappeared and $3CaO{\cdot}Al_2O_3{\cdot}xH_2O$ became the end-product, but the Ca^{2+} and $Al(OH)_4^-$ concentrations were kept constant, which indicated that ion-exchange of I^- with OH^- also happened in the simple dissolution process.

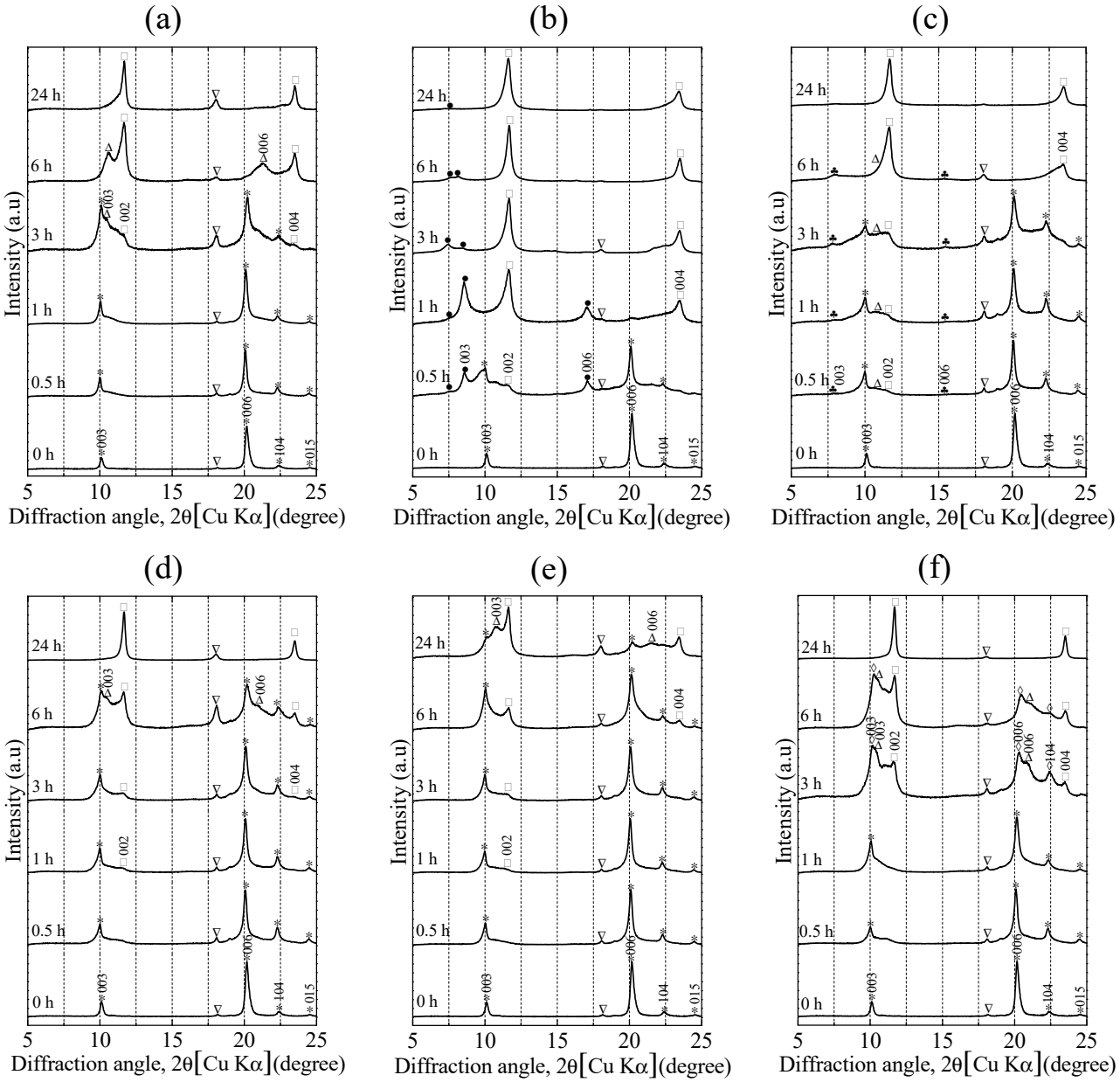

Figure 3. X-ray diffraction patterns of I-hydrocalumite solid residues at different time intervals. (**a**) Blank; (**b**) H_2Cys; (**c**) H_2Asp; (**d**) HGly; (**e**) HPhe; (**f**) HTrp. Symbols indicate, * calcium aluminum iodide oxide hydrate ($3CaO{\cdot}Al_2O_3{\cdot}CaI_2{\cdot}10H_2O$, PDF#42-1474); □ calcium aluminum oxide hydrate ($3CaO{\cdot}Al_2O_3{\cdot}{\times}H_2O$, PDF#02-0083); ∇ unknown; Δ calcium aluminum oxide hydrate ($4CaO{\cdot}Al_2O_3{\cdot}{\times}H_2O$, PDF#02-0077); ◊ calcium aluminum oxide hydrate ($2CaO{\cdot}Al_2O_3{\cdot}6H_2O$, PDF#12-0008), and/or calcium aluminum iodide oxide hydrate ($3CaO{\cdot}Al_2O_3{\cdot}CaI_2{\cdot}H_2O$); • Cys-hydrocalumite; ♣ Asp-hydrocalumite.

Amino acids of H_2Cys, H_2Asp, HGly, HTrp, and HPhe at a concentration of 1.7 mM were used to explore the environmental impact of amino acids on the stability of I-hydrocalumite. As shown in Figure 2d, the equilibrated pH in all series was higher than 12.0, so the -COOH, $-NH_3^+$, and -SH (thiol) functional groups in all amino acids were dissociated because of the p*K*a values of five amino acids. This means H_2Cys, H_2Asp, HGly, HTrp, and HPhe existed in the form Cys^{2-}, Asp^{2-}, Gly^-, Trp^-, and Phe^- under the present pH. Based on the bond length and bond angle of each amino acid molecule, the sizes including length (Å) and width (Å) were estimated [38,39]: glycine (3.9/3.5 Å), L-cysteine (6.4/3.7 Å), L-aspartic acid (6.5/3.5 Å), L-phenylalanine (9.7/4.7 Å), and L-tryptophan (10.9/5.6 Å), so we can clearly distinguish that L-phenylalanine and L-tryptophan had larger molecular sizes. Combing the van der Waals volumes [40] of glycine (48 $Å^3$), L-cysteine (86 $Å^3$), L-aspartic acid (91 $Å^3$), L-phenylalanine (135 $Å^3$), and L-tryptophan (163 $Å^3$), the glycine had the smallest molecular size and L-cysteine was smaller than L-aspartic acid.

In the presence of H_2Cys, at 0.5 h and 1 h, the leaching fraction of I^- corresponded to 74.7% (1.637 mM) and 91.9% (2.016 mM), respectively (Figure 2a). After 24 h, the released concentration was 2.128 mM, corresponding to 97.1% of the original content of I^- in I-hydrocalumite. Therefore, the release rate of I^- was great in the presence of H_2Cys, compared with the blank test at all times; finally, the leaching concentration was larger than 2.003 mM in the blank. From Figure 2e, the decreasing changes in the H_2Cys concentration suggest a possible ion-exchange mechanism of Cys^{2-}, as in Equation (4):

$$Ca_4Al_2(OH)_{12}I_2{\cdot}4H_2O + Cys^{2-} = Ca_4Al_2(OH)_{12}(Cys){\cdot}4H_2O + 2I^- \quad (4)$$

After 0.5 h, the concentration of Cys^{2-} reduced to 0.75 mM, which meant that 0.95 mM Cys^{2-} was immobilized in the solid. According to the charge balance, Cys^{2-} provided 1.9 meq/L negative charges, which were enough to substitute with 1.637 mM I^- from I-hydrocalumite. In addition, the XRD patterns verified the expectation. In Figure 3b, two reflections at d_{003} 10.306 Å (8.58°, 2θ) and 11.694 Å (7.56°, 2θ) appeared after 0.5 h and should be assigned to Cys-hydrocalumite. After 3 h, the d_{003} peak intensity of Cys-hydrocalumite at 8.54° (2θ) decreased and almost disappeared after 24 h, resulting in $3CaO{\cdot}Al_2O_3{\cdot}xH_2O$, which is the main phase. The Ca^{2+} and $Al(OH)_4^-$ concentrations until 6 h, in Figure 2b,c, showed higher values than the blank test, which might suggest the ion-exchanging process destabilized the metallic hydroxide layer of I-hydrocalumite. After 6 h, the decrease in Ca^{2+} and $Al(OH)_4^-$ concentrations were ascribed to the co-precipitation with OH^- to form $3CaO{\cdot}Al_2O_3{\cdot}xH_2O$.

H_2Asp showed a slightly different trend from H_2Cys, while both amino acids were charged to −2 under the present pH conditions. In the presence of H_2Asp, the release rate of I^- was slower than that of the H_2Cys series but larger than the blank test, as shown in Figure 2a. At the suspension times of 0.5 h and 1 h, the released concentrations of I^- were 1.258 mM (57.4%) and 1.426 mM (65.1%), respectively, which were much lower than in the H_2Cys series. After 24 h, 2.087 mM I^- was released, corresponding to 95.2% of the original amount of I^- in I-hydrocalumite. The changes in Asp^{2-} concentrations in Figure 2e show that adsorbed amounts of Asp^{2-} were much smaller than Cys^{2-}. After 0.5 h, the concentration of Asp^{2-} decreased from 1.70 mM to 1.42 mM, so 0.56 meq/L of negative charge were involved in ion-exchange with I^-. In Figure 3c, a phase of Asp-hydrocalumite appeared within 0.5 h with a d_{003} value of 11.305 Å (7.82°, 2θ) and was maintained until 6 h with a small intensity. Therefore, this solid phase changing process also verified the ion-exchange of Asp^{2-} with I^-, as in Equation (5):

$$Ca_4Al_2(OH)_{12}I_2{\cdot}4H_2O + Asp^{2-} = Ca_4Al_2(OH)_{12}(Asp){\cdot}4H_2O + 2I^- \quad (5)$$

In Figure 2b,c, the released Ca^{2+} and $Al(OH)_4^-$ concentrations were always lower than in the blank test, except in the presence of H_2Cys, demonstrating that leaching of I^-

was not caused by only simple dissolution. Thus, the residual 0.698 mM I^- at 0.5 h was ascribed to ion-exchange with OH^- in I-hydrocalumite to form $3CaO{\cdot}Al_2O_3{\cdot}xH_2O$.

As observed in Figure 3b,c, the d_{003} diffraction peaks of Cys/Asp-hydrocalumite finally disappeared after 24 h, but the released fraction of Ca and Al concentrations were kept mostly constant. This means that Cys/Asp-hydrocalumite phases were unstable and changed into a $3CaO{\cdot}Al_2O_3{\cdot}xH_2O$ phase through ion-exchange of Cys^{2-}/Asp^{2-} with OH^-, as in Equation (6):

$$Ca_4Al_2(OH)_{12}(\text{Amino acid}){\cdot}4H_2O + yOH^- = 3CaO{\cdot}Al_2O_3{\cdot}xH_2O + (\text{Amino acid})^{2-} + Ca^{2+} \quad (6)$$

The different performances of H_2Cys and H_2Asp on the release rate of I^- might be caused by their different molecular sizes and the existence of a thiol group (-SH) in H_2Cys. Cys^{2-} possesses a slightly smaller molecule than Asp^{2-} under the same alkaline conditions, which made it easier to enter the interlayer of hydrocalumite.

However, in the HGly and HTrp series, Figure 2a shows a similar amount of released I^- in the blank test within the initial 0.5 h. During the period of 0.5 h to 6 h, the leaching amount of I^- was lower than in the blank. Furthermore, the released amounts of Ca^{2+} (Figure 2b) and $Al(OH)_4^-$ (Figure 2c) were also lower than in the blank. This means that the surface adsorption of Gly^- and Trp^- by electrostatic interaction on hydrocalumite might happen more easily than their intercalation into the $[Ca_2Al(OH)_6]^+$ metallic interlayer. Figure 2e presents the changes in amino acids concentrations. The adsorption of Gly^- and Trp^- on solid phases were always very low over the reaction times, which is consistent with the prediction that only surface adsorption of them happened, rather than intercalation. This phenomenon relates to their properties. HGly has the smallest molecular size among these amino acids, and is dissociated to Gly^- at the presented pH. Therefore, the ion-exchange of Gly^- with I^- appears to be difficult. For HTrp, which possesses a relatively large molecular size, one negative charge, and an aromatic group that made it more difficult to go into the hydrocalumite interlayer by substituting with I^-. After adding 1.7 mM HGly, the phase of I-hydrocalumite was maintained within 6 h but disappeared and transformed into $3CaO{\cdot}Al_2O_3{\cdot}xH_2O$ as the main product after 24 h (Figure 3d). It seems that HGly acted to stabilize I-hydrocalumite a bit longer, compared with no co-existing amino acids. It seems that no d_{003} diffraction peak of Gly-hydrocalumite appeared in small diffraction angles, so the intercalation of HGly did not significantly occur. When HTrp was co-existing with I-hydrocalumite (Figure 3f), the intermediate phase of calcium aluminum oxide hydrate of $2CaO{\cdot}Al_2O_3{\cdot}xH_2O$ (PDF#12-0008), $4CaO{\cdot}Al_2O_3{\cdot}xH_2O$, and $3CaO{\cdot}Al_2O_3{\cdot}xH_2O$ appeared after 3 h. However, the XRD peaks assigned to $2CaO{\cdot}Al_2O_3{\cdot}xH_2O$ seemed to overlap with I-hydrocalumite from 3 h to 6 h.

HPhe showed slightly stronger suppressing effects to release I^- than HGly and HTrp (Figure 2a). HPhe and HTrp belong to aromatic amino acids that have similar molecular sizes and structures, but within 1 h, the concentration of HPhe decreased to 1.04 mM (Figure 2e), indicating that 0.66 mM Phe^- was kept in the solid phase. Combining the solution data with the corresponding XRD patterns, the surface adsorption of Phe^- can be determined. In Figure 3e, $3CaO{\cdot}Al_2O_3{\cdot}xH_2O$ became the main phase after 24 h but I-hydrocalumite in the solid residues was still maintained. It is obvious that I^- was still preserved in hydrocalumite rather than released into the solution. This phenomenon is consistent with the solution results in Figure 2a, indicating the more significantly inhibitory effects of HPhe. Between 1 h and 3 h, the concentration of Phe^- in the solid phase decreased, and after that it became constant. However, after 3 h, the main phase was transformed from I-hydrocalumite to $3CaO{\cdot}Al_2O_3{\cdot}xH_2O$ (Figure 3e), suggesting that HPhe might be likely to be retained on the surface of I-hydrocalumite and $3CaO{\cdot}Al_2O_3{\cdot}xH_2O$. Based on the above results, HPhe and HTrp showed different effects on the leaching of I^- from I-hydrocalumite. HPhe and HTrp have one -COOH group and a side chain with an aromatic group to give it a hydrophobic property. Initially, the ion-exchange and surface adsorption of negatively charged Phe^- and Trp^- are able to occur on I-hydrocalumite. The adsorbed Phe^- and Trp^- may modify the surface properties of I-hydrocalumite from hydrophilic to hydrophobic to some extent [41,42]. Under a high concentration of 1.7 mM of HPhe and

HTrp, more hydrophobic molecules were adsorbed onto the surface rather than stabilized in the interlayer. However, HPhe has a stronger hydrophobic property when Phe^- is adsorbed onto the surface by electrostatic interaction; OH^- in the solution had difficulty in contacting I-hydrocalumite, thus, it might prevent OH^- ion-exchange with I^-.

To ensure the decomposition of I-hydrocalumite, the particle morphologies of solid residues, before and after reaction with different amino acids for 24 h, were observed using SEM and are shown in Figure 4. Figure 4c shows the morphology of I-hydrocalumite solid residue after being suspended in an alkaline solution in the absence of amino acids. A hexagonal structure, irregular structures, and a collapsed layer structure were observed, which are characteristic of typical layered double hydroxides [43]. After suspension in different amino acids solutions, in the H_2Cys (Figure 4d), H_2Asp (Figure 4e), HGly (Figure 4f), and HTrp (Figure 4h) series, there were not only collapsed layer structures, but also aggregation and the frame of a hexagonal structure, suggesting the dissolution of I-hydrocalumite. For HPhe (Figure 4g), the layered structure and clear hexagonal-like morphology still existed, which was consistent with the XRD pattern at 24 h (Figure 3e).

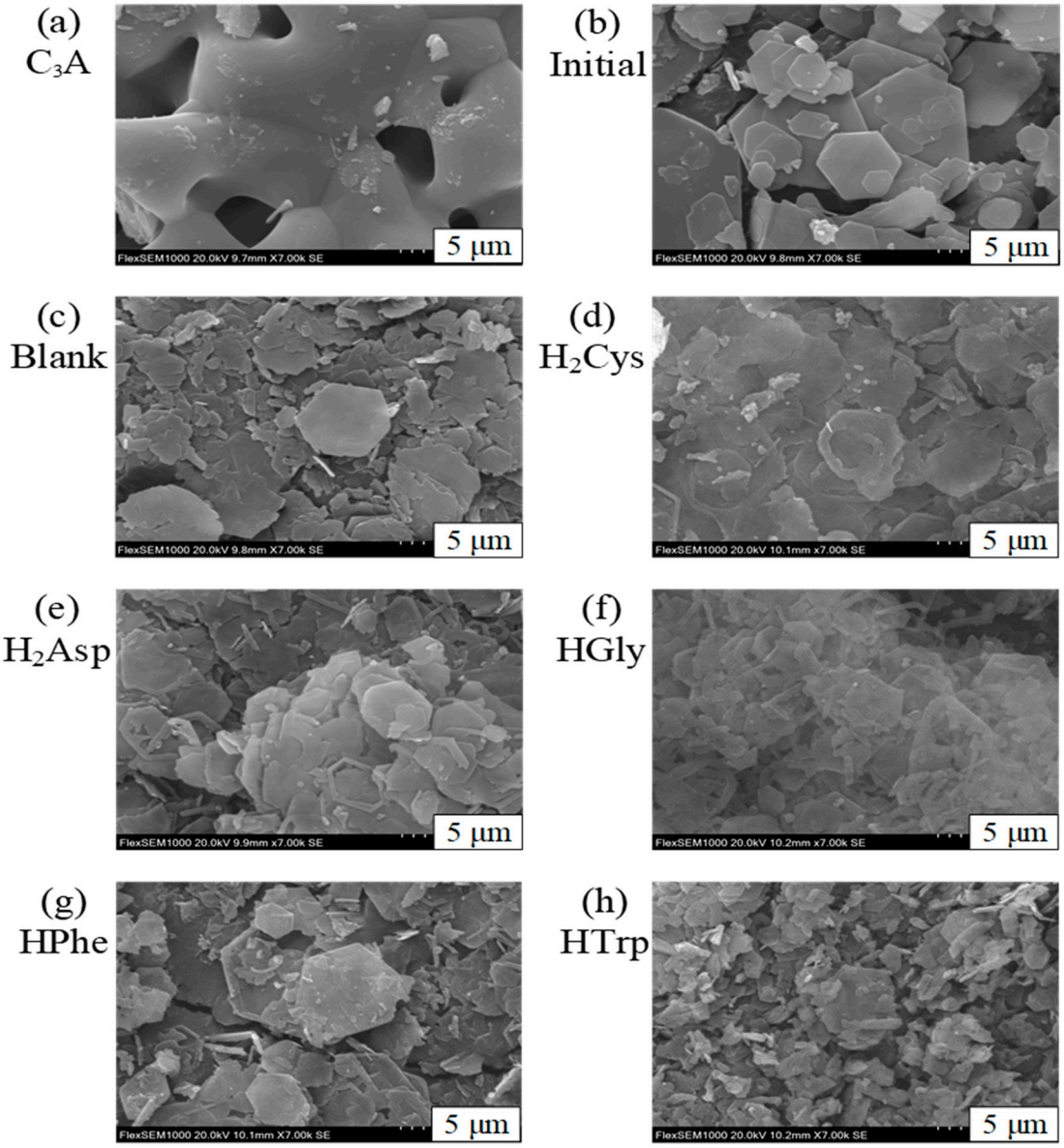

Figure 4. SEM images of (**a**) tricalcium aluminate (C_3A), (**b**) original I-hydrocalumite and solid residues after suspension of I-hydrocalumite in different solutions for 24 h. (**c**) Blank, (**d**) H_2Cys, (**e**) H_2Asp, (**f**) HGly, (**g**) HPhe, and (**h**) HTrp.

Therefore, based on the above results, HGly, HTrp, and HPhe suppressed the dissolution rate of I-hydrocalumite, and HPhe also suppressed the released amount of I^-, while H_2Cys and H_2Asp enhanced the release of I^- from I-hydrocalumite to form other solid phases, but at different rates. Furthermore, a small amount of I-hydrocalumite still existed according to the SEM images, where a hexagonal morphology was maintained.

3.3. Behavior of Amino Acids in I-Hydrocalumite

To explore the different effects between Cys^{2-} and Asp^{2-} on the interaction with I-hydrocalumite, the total formation energies (DE) were calculated following Equations (7) and (8):

$$[Ca_2Al(OH)_6]^+ + 0.5(Asp^{2-}/Cys^{2-}) \rightarrow Ca_2Al(OH)_6 \cdot 0.5(Asp/Cys) \quad (7)$$

$$DE = E(Ca_2Al(OH)_6 \cdot 0.5(Asp/Cys)) - [E([Ca_2Al(OH)_6]^+) + E0.5(Asp^{2-}/Cys^{2-})] \quad (8)$$

where $E(Ca_2Al(OH)_6 \cdot 0.5(Asp/Cys))$, $E([Ca_2Al(OH)_6]^+)$, and $E0.5(Asp^{2-}/Cys^{2-})$ were the calculated energies from DFT.

Considering different configurations of Cys-hydrocalumite and Asp-hydrocalumite, total formation energies were plotted against their interlayer spacings (Figure 5). There was a positive correlation, which indicated that the total formation energies of the system also increased with the increase in interlayer distances. Higher formation energy means a more unstable system. Here, we selected the most stable and most unstable systems, which possessed the lowest and highest total energies, respectively. In Figure 6a, the most stable configuration $Ca_4Al_2(OH)_{12}$·Asp (0 kJ/mol) showed an interlayer distance of 7.34 Å with one Ca-O bond and seven hydrogen bonds in one unit cell. In Figure 6b, the most unstable system $Ca_4Al_2(OH)_{12}$·Asp (71.2 kJ/mol) showed a layer spacing of 8.57 Å with one Ca-O bond and six hydrogen bonds between the metal hydroxide layers and Asp^{2-} in one unit cell. For H_2Cys, the most stable system of $Ca_4Al_2(OH)_{12}$·Cys with a formation energy of 0 kJ/mol showed a 7.22 Å interlayer spacing including one Ca-O and three hydrogen bonds between metal hydroxide layers and Cys^{2-} (Figure 6d). The most unstable system, $Ca_4Al_2(OH)_{12}$·Cys, showed 8.92 Å of interlayer distance in 85.6 kJ/mol (Figure 6e). From these results, the simulations predicted a much lower interlayer spacing than the observed XRD results (Figure 3b,c). As can be confirmed, the water molecules can cause the expansion of the interlayer spacings in experimental results [44,45]. Thus, we considered a new system, which included one water molecule in one unit cell of hydrocalumite including Asp^{2-}, as shown in Figure 6c. In the system of $Ca_4Al_2(OH)_{12}Asp \cdot 4H_2O$, the corresponding interlayer spacing was 7.99 Å under the lowest formation energy of 0 kJ/mol, which indicated that the presence of water molecules can affect the expansion of the interlayer distances. Therefore, in a real system, the most stable state is possibly overlapped by the d_{003} peak in XRD, assigned to $3CaO \cdot Al_2O_3 \cdot CaI_2 \cdot 10H_2O$ in 11.6°, 2θ. The XRD diffraction peaks at 8.54° (2θ), 7.61° (2θ), and 7.92° (2θ) in Figure 3b,c might be caused by the different water molecule numbers included in each system, affecting the configurations of Asp^{2-} and Cys^{2-} in the metallic hydroxide layer. Another factor might be related to the difference in the basal layer charge densities, which has been confirmed through the positive correlation relationship between them [46].

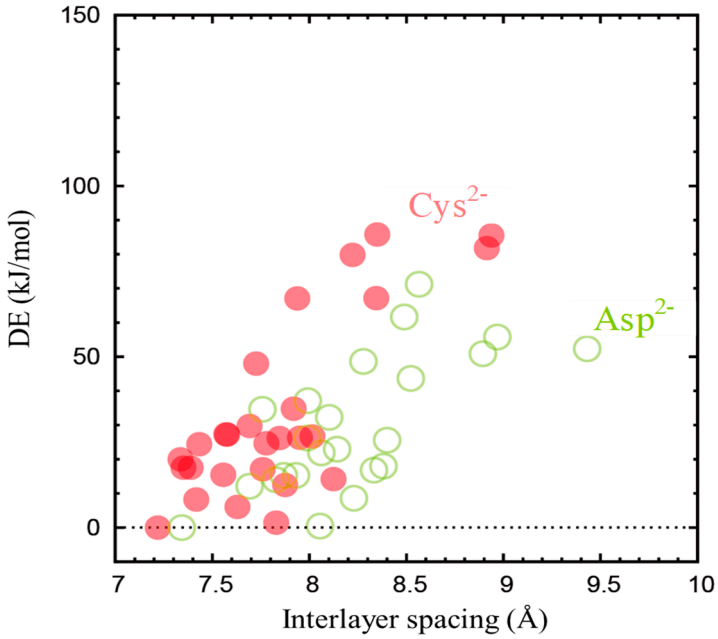

Figure 5. Energy difference (DE) plotted against interlayer spacing for hydrocalumite(Asp/Cys) after intercalation of Asp^{2-} (green circles) and Cys^{2-} (red circles).

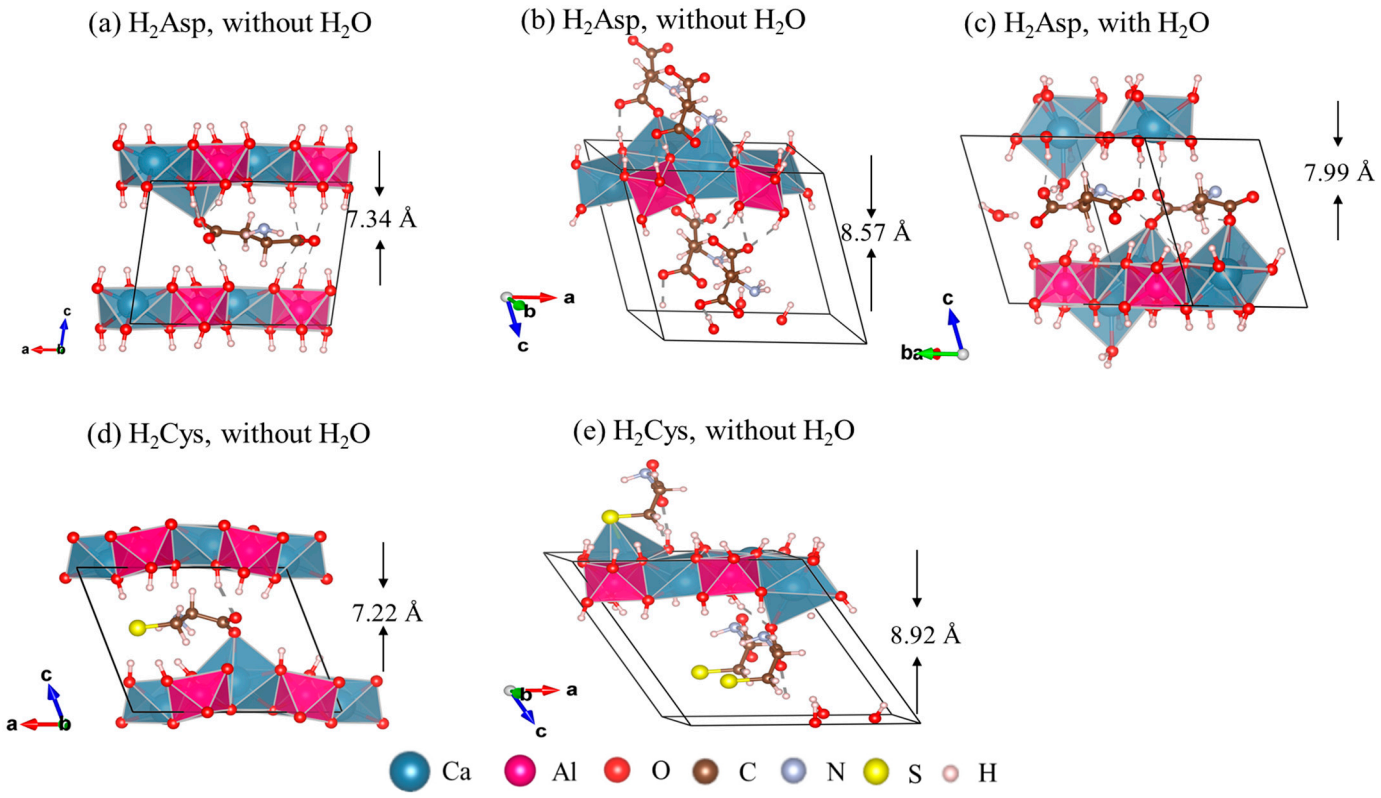

Figure 6. Simulated results of H_2Asp and H_2Cys in a model of Ca_2Al-LDH. The dashed and solid lines indicate hydrogen bonds and Ca-O bonds, respectively. (**a**) Most stable, 0 kJ/mol; (**b**) most unstable, 71.2 kJ/mol; (**c**) most stable, 0 kJ/mol; (**d**) most stable, 0 kJ/mol; (**e**) most unstable, 85.6 kJ/mol.

4. Conclusions

The interaction of five selected amino acids with iodide intercalated hydrocalumite was investigated by solid and solution chemistry integrated with DFT simulations. I-hydrocalumite was very fragile and caused dissolution, even at pH 12.0. After being suspended in amino acids solutions, the main factors that caused the release of I^- were divided into ion-exchange and simple dissolution. H_2Cys and H_2Asp accelerated the releasing rate of I^- through ion-exchange between Cys^{2-}/Asp^{2-} and I^-. Using XRD, expanded d_{003} spacings were observed, which was different from the other three amino acids. However, the effects of Cys^{2-} and Asp^{2-} on the ion-exchange with I^- in hydrocalumite and the stability of I-hydrocalumite were different. Asp^{2-} maintained a structure of I-hydrocalumite for a longer time than Cys^{2-}, and Cys-intercalated hydrocalumite showed one smaller d_{003} spacing than Asp-intercalated hydrocalumite in the XRD patterns. This was also verified by DFT simulations. DFT simulations also confirmed that the interlayer spacings might be strongly influenced by the presence of water molecules and water numbers. There are interaction forces between amino acids and hydrocalumite in which the hydrogen and Ca-O bonds contributed to their configurations, but the Asp/Cys-hydrocalumite system was still unstable. In the presence of HGly, HTrp, and HPhe, the simple dissolution and ion-exchange with OH^- contributed to I-hydrocalumite decomposition. Moreover, HPhe showed slight inhibitory effects on the release of I^- by surface adsorption. Thus, some organic matter that is negatively charged with a large molecule and less affinity than I^- might make hydrocalumite stable. Hence, for iodide isotope stabilization in cementitious materials, I-hydrocalumite may be formed, but its stabilization is strongly influenced by the geochemical environment.

Supplementary Materials: The following are available online at https://www.mdpi.com/article/10.3390/min11080836/s1, Figure S1: Construction of amino acids-hydrocalumite model in DFT simulation.

Author Contributions: Conceptualization, M.W. and K.S.; methodology, M.W. and H.A.; software, H.A.; formal analysis, M.W.; resources, K.S.; data curation, M.W.; writing—original draft preparation, M.W.; writing—review and editing, M.W. and K.S.; visualization, H.A.; supervision, K.S.; project administration, K.S.; funding acquisition, K.S. All authors have read and agreed to the published version of the manuscript.

Funding: This research was funded by Japan Society for the Promotion of Science (JSPS) KAKENHI research grants (Grant Nos. JP19H00883) and Kyushu University Progress 100 (Grant Nos. Invitation program for top global researchers) Strategic partnership acceleration (FY2020-2022).

Institutional Review Board Statement: Not applicable.

Informed Consent Statement: Not applicable.

Data Availability Statement: The data presented in this study are available in this article.

Acknowledgments: The authors wish to acknowledge the Research Institute for Information Technology at Kyushu University, the China Scholarship Council which provide scholarship for M.W. We also want to express our appreciation to the editors of Minerals and reviewers.

Conflicts of Interest: The authors declare no conflict of interest.

References

1. Avalos, N.M.; Varga, T.; Mergelsberg, S.T.; Silverstein, J.A.; Saslow, S.A. Behavior of iodate substituted ettringite during aqueous leaching. *Appl. Geochem.* **2021**, *125*, 104863. [CrossRef]
2. Leisinger, S.M.; Lothenbach, B.; Le Saout, G.; Johnson, C.A. Thermodynamic modeling of solid solutions between monosulfate and monochromate $3CaO{\cdot}Al_2O_3{\cdot}Ca[(CrO_4)_x(SO_4)_{1-x}]{\cdot}nH_2O$. *Cem. Concr. Res.* **2012**, *42*, 158–165. [CrossRef]
3. Guo, B.; Xiong, Y.; Chen, W.; Saslow, S.A.; Kozai, N.; Ohnuki, T.; Dabo, I.; Sasaki, K. Spectroscopic and first-principles investigations of iodine species incorporation into ettringite: Implications for iodine migration in cement waste forms. *J. Hazard. Mater.* **2020**, *389*, 121880. [CrossRef]
4. Toyohara, M.; Kaneko, M.; Ueda, H.; Mitsutsuka, N.; Fujihara, H.; Murase, T.; Saito, N. Iodine sorption onto mixed solid alumina cement and calcium compounds. *J. Nucl. Sci. Technol.* **2000**, *37*, 970–978. [CrossRef]

5. Toyohara, M.; Kaneko, M.; Mitsutsuka, N.; Fujihara, H.; Saito, N.; Murase, T. Contribution to understanding iodine sorption mechanism onto mixed solid alumina cement and calcium compounds. *J. Nucl. Sci. Technol.* **2002**, *39*, 950–956. [CrossRef]
6. Gao, H.; Cao, R.; Xu, X.; Xue, J.; Zhang, S.; Hayat, T.; Alharbi, N.S.; Li, J. Surface area-and structure-dependent effects of LDH for highly efficient dye removal. *ACS Sustain. Chem. Eng.* **2018**, *7*, 905–915. [CrossRef]
7. Audi, G.; Bersillon, O.; Blachot, J.; Wapstra, A.H. The NUBASE evaluation of nuclear and decay properties. *Nucl. Phys.* **2003**, *729*, 3–128. [CrossRef]
8. Iglesias, L.; Walther, C.; Medina, F.; Hölzer, A.; Neumann, A.; Lozano-Rodriguez, M.J.; Álvarez, M.G.; Torapava, N. A comprehensive study on iodine uptake by selected LDH phases via coprecipitation, anionic exchange and reconstruction. *J. Radioanal. Nucl. Chem.* **2016**, *307*, 111–121. [CrossRef]
9. Theiss, F.L.; Ayoko, G.A.; Frost, R.L. Iodide removal using LDH technology. *Chem. Eng. J.* **2016**, *296*, 300–309. [CrossRef]
10. Haruguchi, Y.; Higuchi, S.; Obata, M.; Sakuragi, T.; Takahashi, R.; Owada, H. A study on Iodine Release Behavior from Iodine-Immobilizing Cement Solid. *MRS Online Proc. Libr.* **2013**, *1518*, 85–90. [CrossRef]
11. Atkins, M.; Glasser, F.P.; Kindness, A. Cement hydrate phase: Solubility at 25 °C. *Cem. Concr. Res.* **1992**, *22*, 241–246. [CrossRef]
12. Ochs, M.; Mallants, D.; Wang, L. *Radionuclide and Metal Sorption on Cement and Concrete*; Springer: Berlin, Germany, 2016. [CrossRef]
13. Aimoz, L.; Wieland, E.; Taviot-Guého, C.; Dähn, R.; Vespa, M.; Churakov, S.V. Structural insight into iodide uptake by AFm phases. *Environ. Sci. Technol.* **2012**, *46*, 3874–3881. [CrossRef] [PubMed]
14. Dai, J.L.; Zhang, M.; Hu, Q.H.; Huang, Y.Z.; Wang, R.Q.; Zhu, Y.G. Adsorption and desorption of iodine by various Chinese soils: II. Iodide and iodate. *Geoderma* **2009**, *153*, 130–135. [CrossRef]
15. Emerson, H.P.; Xu, C.; Ho, Y.; Zhang, S.; Schwehr, K.A.; Lilley, M.; Kaplan, D.I.; Santschi, P.H.; Powell, B.A. Geochemical controls of iodine uptake and transport in Savannah River Site subsurface sediments. *Appl. Geochem.* **2014**, *45*, 105–113. [CrossRef]
16. Xu, C.; Kaplan, D.I.; Zhang, S.; Athon, M.; Ho, Y.; Li, H.; Yeager, C.M.; Schwehr, K.A.; Grandbois, R.; Wellman, D. Radioiodine sorption/desorption and speciation transformation by subsurface sediments from the Hanford Site. *J. Environ. Radioactiv.* **2015**, *139*, 43–55. [CrossRef] [PubMed]
17. Li, J.; Zhou, H.; Wang, Y.; Xie, X.; Qian, K. Sorption and speciation of iodine in groundwater system: The roles of organic matter and organic-mineral complexes. *J. Contam. Hydrol.* **2017**, *201*, 39–47. [CrossRef] [PubMed]
18. Nedyalkova, L.; Lothenbach, B.; Geng, G.; Mäder, U.; Tits, J. Uptake of iodide by calcium aluminate phases (AFm phases). *Appl. Geochem.* **2020**, *116*, 104559. [CrossRef]
19. Gao, K.; Chen, G.; Wu, D. A DFT study on the interaction between glycine molecules/radicals and the (8, 0) SiCNT. *Phys. Chem. Chem. Phys.* **2014**, *16*, 17988–17997. [CrossRef]
20. Ma, B.; Fernandez-Martinez, A.; Grangeon, S.; Tournassat, C.; Findling, N.; Claret, F.; Koishi, A.; Marty, N.C.; Tisserand, D.; Bureau, S. Evidence of multiple sorption modes in layered double hydroxides using Mo as structural probe. *Environ. Sci. Technol.* **2017**, *51*, 5531–5540. [CrossRef] [PubMed]
21. Kresse, G.; Joubert, D. From ultrasoft pseudopotentials to the projector augmented-wave method. *Phys. Rev. B* **1999**, *59*, 1758. [CrossRef]
22. Blöchl, P.E. Projector augmented-wave method. *Phys. Rev. B* **1994**, *50*, 17953. [CrossRef]
23. Kresse, G.; Hafner, J. Ab initio molecular dynamics for open-shell transition metals. *Phys. Rev. B* **1993**, *48*, 13115. [CrossRef]
24. Kresse, G.; Furthmüller, J. Efficient iterative schemes for ab initio total-energy calculations using a plane-wave basis set. *Phys. Rev. B* **1996**, *54*, 11169. [CrossRef] [PubMed]
25. Kresse, G.; Furthmüller, J. Efficiency of ab-initio total energy calculations for metals and semiconductors using a plane-wave basis set. *Comput. Mater. Sci.* **1996**, *6*, 15–50. [CrossRef]
26. Perdew, J.P.; Burke, K.; Ernzerhof, M. Generalized gradient approximation made simple. *Phys. Rev. Lett.* **1996**, *77*, 3865. [CrossRef] [PubMed]
27. Ernzerhof, M.; Perdew, J.P.; Burke, K. Coupling-constant dependence of atomization energies. *Int. J. Quantum Chem.* **1998**, *64*, 285–295. [CrossRef]
28. Perdew, J.P.; Ruzsinszky, A.; Csonka, G.I.; Vydrov, O.A.; Scuseria, G.E.; Constantin, L.A.; Zhou, X.; Burke, K. Restoring the density-gradient expansion for exchange in solids and surfaces. *Phys. Rev. Lett.* **2008**, *100*, 136406. [CrossRef] [PubMed]
29. Grimme, S.; Ehrlich, S.; Goerigk, L. Effect of the damping function in dispersion corrected density functional theory. *J. Comput. Chem.* **2011**, *32*, 1456–1465. [CrossRef]
30. Grimme, S.; Antony, J.; Ehrlich, S.; Krieg, H. A consistent and accurate ab initio parametrization of density functional dispersion correction (DFT-D) for the 94 elements H-Pu. *J. Chem. Phys.* **2010**, *132*, 154104. [CrossRef]
31. William, D.C. *Fundamentals of Materials Science and Engineering: An Interactive*; Wiley: London, UK, 2001.
32. Arunan, E.; Desiraju, G.R.; Klein, R.A.; Sadlej, J.; Scheiner, S.; Alkorta, I.; Clary, D.C.; Crabtree, R.H.; Dannenberg, J.J.; Hobza, P.; et al. Definition of the hydrogen bond (IUPAC Recommendations 2011). *Pure Appl. Chem.* **2011**, *83*, 1637–1641. [CrossRef]
33. Sacerdoti, M.; Passaglia, E. Hydrocalumite from Latium, Italy: Its crystal structure and relationship with related synthetic phases. *Neues Jahrbuch für Mineralogie Monatshefte* **1988**, *10*, 462–475.
34. Ong, S.P.; Richards, W.D.; Jain, A.; Hautier, G.; Kocher, M.; Cholia, S.; Gunter, D.; Chevrier, V.L.; Persson, K.A.; Ceder, G. Python Materials Genomics (pymatgen): A robust, open-source python library for materials analysis. *Comput. Mater. Sci.* **2013**, *68*, 314–319. [CrossRef]

35. Momma, K.; Izumi, F. VESTA 3 for three-dimensional visualization of crystal, volumetric and morphology data. *J. Appl. Crystallogr.* **2011**, *44*, 1272–1276. [CrossRef]
36. Sánchez-Herrero, M.J.; Fernández-Jiménez, A.; Palomo, A. Alkaline hydration of tricalcium aluminate. *J. Am. Chem. Soc.* **2012**, *95*, 3317–3324. [CrossRef]
37. Rapin, J.P.; Walcarius, A.; Lefevre, G.; Francois, M. A double-layered hydroxide, $3CaO{\cdot}Al_2O_3{\cdot}CaI_2{\cdot}10H_2O$. *Acta Crystallogr. Sect. C Cryst. Struct.Commun.* **1999**, *55*, 1957–1959. [CrossRef]
38. Ching, C.; Hidajat, K.; Uddin, M. Evaluation of equilibrium and kinetic parameters of smaller molecular size amino acids on KX zeolite crystals via liquid chromatographic techniques. *Sep. Sci. Technol.* **1989**, *24*, 581–597. [CrossRef]
39. Weast, C.; Astle, M. *Handbook of Chemistry and Physics*; Table D-190; CRC Press: Boca Raton, FL, USA, 1979.
40. Nölting, B. *Physical Interactions That Determine the Properties of Proteins*; Springer: Berlin, Germany, 2006.
41. Silvério, F.; Dos Reis, M.J.; Tronto, J.; Valim, J.B. Sorption of aspartic and glutamic aminoacids on calcined hydrotalcite. *SpringerPlus* **2013**, *2*, 211. [CrossRef]
42. Khenifi, A.; Derriche, Z.; Mousty, C.; Prévot, V.; Forano, C. Adsorption of glyphosate and glufosinate by Ni_2AlNO_3 layered double hydroxide. *Appl. Clay Sci.* **2010**, *47*, 362–371. [CrossRef]
43. Choi, W.; Ghorpade, P.A.; Kim, K.; Shin, J.; Park, J. Properties of synthetic monosulfate as a novel material for arsenic removal. *J. Hazard. Mater.* **2012**, *227*, 402–409. [CrossRef]
44. Yan, D.; Lu, J.; Wei, M.; Ma, J.; Evans, D.G.; Duan, X. A combined study based on experiment and molecular dynamics: Perylene tetracarboxylate intercalated in a layered double hydroxide matrix. *Phys. Chem. Chem. Phys.* **2009**, *11*, 9200–9209. [CrossRef]
45. Grégoire, B.; Erastova, V.; Geatches, D.L.; Clark, S.J.; Greenwell, H.C.; Fraser, D.G. Insights into the behaviour of biomolecules on the early Earth: The concentration of aspartate by layered double hydroxide minerals. *Geochim. Cosmochim. Acta* **2016**, *176*, 239–258. [CrossRef]
46. Zhang, Y.; Liu, X.; Zhang, C.; He, M.; Lu, X. Interlayer structures and dynamics of arsenate and arsenite intercalated layered double hydroxides: A first principles study. *Minerals* **2017**, *7*, 53. [CrossRef]